NeuroImage: Clinical 37 (2023) 103291

Contents lists available at ScienceDirect

NeuroImage: Clinical

journal homepage: www.elsevier.com/locate/ynicl

A presurgical voxel-wise predictive model for cerebellar mutism syndrome in children with posterior fossa tumors

Wei Yang [a,2], Yiming Li [b,2], Zesheng Ying [a], Yingjie Cai [a], Xiaojiao Peng [a], HaiLang Sun [a], Jiashu Chen [a], Kaiyi Zhu [c,d], Geli Hu [e], Yun Peng [f,1,*], Ming Ge [a,*,1]

[a] Department of Neurosurgery, Beijing Children's Hospital, Capital Medical University, National Center for Children's Health, Beijing 100045, China
[b] Department of Neurosurgery, Beijing Tiantan Hospital, Capital Medical University, Beijing 100070, China
[c] Department of Cardiology, Shanxi Bethune Hospital, Shanxi Academy of Medical Sciences, Tongji Shanxi Hospital, Third Hospital of Shanxi Medical University, Taiyuan 030032, China
[d] Tongji Hospital, Tongji Medical College, Huazhong University of Science and Technology, Wuhan 030032, China
[e] Department of Clinical and Technical Support, Philips Healthcare, Beijing 100600, China
[f] Department of Image Center, Beijing Children's Hospital, Capital Medical University, National Center for Children's Health, Beijing 100045, China

ARTICLE INFO

Keywords:
Lesion-symptom mapping
Cerebellar mutism syndrome
Predictive model

ABSTRACT

Background: This study aimed to investigate cerebellar mutism syndrome (CMS)-related voxels and build a voxel-wise predictive model for CMS.

Methods: From July 2013 to January 2022, 188 pediatric patients diagnosed with posterior fossa tumor were included in this study, including 38 from a prospective cohort recruited between 2020 and January 2022, and the remaining from a retrospective cohort recruited in July 2013-Aug 2020. The retrospective cohort was divided into the training and validation sets; the prospective cohort served as a prospective validation set. Voxel-based lesion symptoms were assessed to identify voxels related to CMS, and a predictive model was constructed and tested in the validation and prospective validation sets.

Results: No significant differences were detected among these three data sets in CMS rate, gender, age, tumor size, tumor consistency, presence of hydrocephalus and paraventricular edema. Voxels related to CMS were mainly located in bilateral superior and inferior cerebellar peduncles and the superior part of the cerebellum. The areas under the curves for the model in the training, validation and prospective validation sets were 0.889, 0.784 and 0.791, respectively.

Conclusions: Superior and inferior cerebellar peduncles and the superior part of the cerebellum were related to CMS, especially the right side, and voxel-based lesion-symptom analysis could provide valuable predictive information before surgery.

1. Introduction

Posterior fossa tumor is one of the most common pediatric tumor types, and about a quarter of the affected children suffer from cerebellar mutism syndrome (CMS) after surgery (Khan et al., 2021; Ostrom et al., 2021; Robertson et al., 2006; Toescu et al., 2018). CMS features transient mutism, hypotonia, emotional dysregulation, and cognitive impairment (Catsman-Berrevoets and Aarsen, 2010; Gudrunardottir et al., 2016). Despite recovery from mutism after a period-of time, low speed speech, motor dysfunction and cognitive impairment are still predominant issues in children with CMS in the long run (Cámara et al., 2020; Grieco et al., 2020; Steinbok et al., 2003; Wibroe et al., 2021).

So far, the mechanism of CMS remains unclear. Previous reports have identified some risk factors for CMS, including midline location, medulloblastoma (MB), gender, age, tumor size, hydrocephalus, and surgical route (Catsman-Berrevoets et al., 1999; Doxey et al., 1999; Gora et al., 2017; Khan et al., 2021; Korah et al., 2010; Pols et al., 2017). However, the roles of gender, hydrocephalus, tumor size, and surgical route remain controversial, while midline location and MB have been consistently considered to be associated with CMS (Khan et al., 2021;

* Corresponding authors.
E-mail addresses: ppengyun@hotmail.com (Y. Peng), ming_ge@126.com (M. Ge).
[1] These authors contributed equally as corresponding authors.
[2] These authors contributed equally as first authors.

https://doi.org/10.1016/j.nicl.2022.103291
Received 20 September 2022; Received in revised form 4 December 2022; Accepted 12 December 2022
Available online 13 December 2022

Pettersson et al., 2022). Basically, most of the MB are located at the midline location (Pettersson et al., 2022). Moreover, many studies have demonstrated the significant role of tumor location in the development of CMS (Ashida et al., 2021; Pettersson et al., 2022). However, the description of the tumor location was brief in previous studies. In most cases, tumor location was classified into midline location and lateral location (Gora et al., 2017; Küpeli et al., 2011), and in some cases, it was divided into the vermis, fourth ventricle, and cerebellar hemisphere (Grønbæk et al., 2021; Robertson et al., 2006). Generally, the midline location was associated with an increased risk of CMS, whereas the hemisphere location with lower risk of CMS (Pettersson et al., 2022). However, these descriptions of tumor location were based on the naked eye's judgment and were not precise. Sometimes, it is difficult to classify the tumor into midline or lateral location directly, especially for giant tumors originating from the cerebellar hemisphere nearing the midline and extending to the midline. Although diverse measures have been adopted in surgical practice to avoid CMS, it still occurs inevitably. The critical effect of tumoral location on CMS development cannot be overlooked.

Lesion to symptom mapping (LSM) is a primary tool for understanding the association of brain structure with its function. Different from functional MRI analyses that correlate activated brain regions with behavior, LSM exploits lesion areas and behavior outcomes in patients to generate maps between lesion voxels and behavior evaluation. Traditional LSM is based on the subtraction of overlap from two patient groups, with no statistical test. Since Bates (Bates et al., 2003) proposed modern LSM with statistical analysis, the method has been extensively exploited in cognitive studies. However, in previous modern LSM techniques, each voxel was independently assessed (also termed mass-univariate LSM), which results in systemic statistical bias (Kimberg et al., 2007; Nachev, 2015; Rudrauf et al., 2008). In the mass-univariate approach, the association of lesion status with behavioral performance is examined only one voxel at a time. A shortcoming of such approach is that data pertaining to the spatial associations of a given voxel with neighboring voxels are not taken into consideration (de Haan and Karnath, 2018). Recently, multivariate LSM analysis was developed, overcoming the limitations of mass-univariable LSM. Sparse canonical correlation analysis (SCCAN) for neuroimaging is an algorithm applied in Lesion to Symptom Mapping in R (LESYMAP), which can perform LSM analysis with the multivariate strategy. It has been demonstrated to outperform previous univariate analysis (McMillan et al., 2014; Pustina et al., 2018; Sperber and Karnath, 2017; Zhang et al., 2014).

In this study, a retrospective cohort of children with posterior fossa tumors was examined. We aimed to assess the association of tumor location with CMS in children with posterior fossa tumors. Additionally, we built a predictive model based on LSM data. We hypothesized that LSM can predict CMS if reflecting the actual correlations between anatomical structures and behavior outcomes.

2. Materials and methods

2.1. Patients

We included a retrospective cohort (from July 2013 to August 2020) and a prospective cohort (September 2020–January 2022). Children administered posterior fossa surgery with definite brain tumors in The Department of Pathology at Beijing Children's Hospital were enrolled in this study. Inclusion criteria were: 1) 0–18 years of age; 2) diagnosis of posterior fossa tumors and tumor removal surgery; 3) definite diagnosis of CMS or non-CMS. Exclusion criteria were: 1) incomplete medical records; 2) missing MRI data or corrupted MR images. The patients were regularly followed up at 3 to 6-month intervals by phone or at our outpatient center. Clinicodemographic variables, including gender, age, tumor size, hydrocephalus, and pathology, were retrieved from medical records. The pediatric cases were assigned to two groups based on CMS occurrence. This study was approved by our institutional review board. Informed consent was waived for the retrospective cohort, and was obtained from the patients' parents for the prospective cohorts, in accordance with the Declaration of Helsinki.

2.2. Definition of CMS and clinical variables

CMS was defined as mutism or severely reduced speech after surgery. Other symptoms might emerge simultaneously, including hypotonia, dysphagia, irritability, and involuntary movement. Mutism duration was defined as the time from mutism to when the patient could speak at least one Chinese character, which was acquired through regular follow-up. The tumor consistency was evaluated with a presurgical MRI and the tumor with a cystic part <50 % of the total volume was defined as a solid tumor (Yang et al., 2022).

2.3. MR image acquisition and lesion mask

MR imaging in the retrospective cohort was carried out on a 3.0 T Discovery 750 scanner (GE healthcare, Milwaukee, Wisconsin) with an 8-channel head coil (voxel size, $0.6 \times 0.6 \times 5\ mm^3$). The prospective cohort was examined on a 3.0 T Ingenia CX scanner (Philips Healthcare, Best, the Netherlands) with a 32-channel head coil (voxel size, $1 \times 1 \times 1\ mm^3$). All images were acquired preoperatively.

Tumors were delineated manually on T1W images with ITK-SNAP (https://www.itksnap.org) by a senior neurosurgeon (Dr. Zesheng Ying). T2FLAIR and T2W scans were utilized as reference images. Peritumoral edema areas were not included in the mask. A neuroradiologist (Dr. Yun Peng) checked tumor boundaries. Both the neurosurgeon and neuroradiologist were blinded to the CMS status. Any disagreement was resolved by consensus. Subsequently, scan images and lesion maps were normalized into the Montreal Neurological Institute (MNI) space using Clinical Toolbox (https://www.nitrc.org/projects/clinicaltbx) for statistical parametric mapping (SPM12, Wellcome Department of Neuroscience, London, UK; https://www.fil.ion.ucl.ac.uk/spm/software/spm12/).

The normalized the image were visually checked and images that were not well merged with standardized MNI image were exclude. Then, two lesion overlap mappings were created with the normalized lesion masks for CMS and non-CMS groups.

2.4. Subtraction analysis

A lesion probability map of CMS and non-CMS group patients were generated using SPM according to the formulations: $p = N/M$. The N represented the number of patients overlapped at the corresponding voxel, and M represented the total number of patients in the related group. And then, the non-CMS probability map is subtracted from the CMS probability map to generate the subtraction map.

2.5. Voxel based lesion-symptom analysis

Normalized lesion masks, CMS labels, and CMS grades were integrated to a dataset for voxel-based lesion symptom analysis (VLSM) via LESYMAP (https://github.com/dorianps/LESYMAP), which uses SCCAN to identify the pattern of normalized voxel weights most correlated with concerned behavior. Compared with the traditional mass-univariable VLSM, SCCAN is a novel multivariable approach with all voxels jointly considered in a single model. This method can overcome the limitations of mass-univariable VLSM, including the associations of neighboring voxels, variation of statistical power across the brain map, etc. VLSM analysis is restricted to voxels in which 3 or more patients showed damage, excluding regions with sparse coverage in the cohort (Khan et al., 2021). Each lesion voxel was assigned a weight ranging between 0 and 1; the higher the value, the higher the CMS occurrence. The voxel weights obtained were color-coded and overlaid onto the brain template for display. Statistical analysis of lesion anatomy was

based on the Anatomical Automatic Labeling (AAL) and Natbrainlab atlases (Catani and Thiebaut de Schotten, 2008; Rolls et al., 2020). Finally, a color-coded VLSM map indicating the engaged CMS regions was built. MNI coordinates for the regions with lesion-overlapping in most patients are shown in Table 2.

2.6. Model construction and predictive value assessment

The retrospective cohort was divided into the training and validation sets based on enrollment time. The training cohort was utilized for model construction with LESYMAP, adopting the SCCAN method. A fourfold cross-validation was used to optimize the performance of the predictive model. Then, the optimized predictive model was applied to predict the CMS status in the validation and prospective validation sets.

2.7. Statistical analysis

Statistical analysis was performed with SPSS (IBM SPSS Statistics for Windows, Version 21.0; IBM, Armonk, NY, USA). Descriptive statistics was used to depict clinicodemographic features. Continuous variables were compared by the Kruskal-Wallis test, and category variables by the Chi squared test. Statistical significance was defined as $p < 0.05$. Areas under the receiver operating characteristic (ROC) curves (AUCs) were determined to quantify the performance of the model in the three sets.

3. Results

3.1. Demographic data

Totally 188 participants were analyzed, including 33.5 % (63/188) who were diagnosed with CMS after posterior fossa surgery. Of the 188 participants, 150 and 38 were enrolled in the retrospective and prospective cohorts, respectively. One hundred and two of the retrospective cohort was included in the training set, while the remaining participants and the prospective cohort constituted the validation sets. The clinicodemographic features of the three sets are summarized in Table 1. The median age of the participants was 5.1 [3.0, 7.9] years, and males comprised 60.1 % (113/188) of the total population. MB comprised 39.4 % (74/188), and ependymoma 12.8 % (24/188). The other pathology types, comprising 47.9 % (90/188) of the total, include astrocytoma 59, ganglioglioma 9, atypical teratoid/rhabdoid tumor 6, diffuse midline glioma 3, and others types 13 (including germ cell tumors 1, meningioma 1, choroid plexus papilloma 2, vascular malformation 1, dermoid cyst or epidermoid cyst 2, and other embryonal tumors 6).

The overall CMS incidence was 33.5 % (63/188). Nine cases with loss of speech could not be classified into mild or severe CMS because of unclear mutism duration. Six cases had no follow-up data for mutism duration.

Comparisons of the three data sets showed no significant differences in gender, age, tumor size, tumor consistency, hydrocephalus, paraventricular edema, and presurgical ventriculoperitoneal shunt among the three sets. Significant differences were detected in surgical route ($p < 0.001$), the extent of resection ($p = 0.045$) and pathology ($p = 0.006$), as shown in Table 1.

3.2. Comparison of CMS and non-CMS group

No significant difference was found in volumes of tumors (non-CMS: 7372.0 [4099.0, 12797.0] vs CMS: 6030.0 [4399.5, 9256.0], $p = 0.557$), rate of presurgical VP shunt (non-CMS: 8.8 % vs CMS: 15.9 %, $p = 0.227$) and gross total resection (non-CMS: 88.8 % vs CMS:82.5 %, $p = 0.334$) between the CMS and non-CMS groups. Male gender (non-CMS: 52.8 % vs CMS:74.6, $p = 0.006$), solid tumor (non-CMS: 79.2 % vs CMS: 98.4 %, $p = 0.001$), presence of hydrocephalus (non-CMS: 41.6 % vs CMS: 60.3 %, $p = 0.023$) and paraventricular edema (non-CMS: 53.6 % vs CMS: 73.0 %, $p = 0.016$), surgical routes ($p = 0.001$) and pathology ($p < 0.001$) were statistically associated with CMS, as shown in Table 2.

4. VLSM analysis results

4.1. Lesion mapping

Lesion overlaps of the 102 cases in the training set are displayed in Fig. 1 for descriptive purpose. The regions with maximum overlap ($n = 102$) were mainly located in the lower center of the cerebellum, covering cerebellar peduncle and dentate nucleus areas (Fig. 1). A subtraction probability map was generated by subtract non-CMS probability map from CMS probability map (Fig. 2). The threshold was set as > 0.2, which means voxels in CMS probability map with greater rate by 20 %

Table 1
Summary of clinical features among the three sets.

		Overall (N = 188)	Training (N = 102)	Validation (N = 48)	Prospective (N = 38)	p value
Group, n (%)	Non-CMS	125 (66.5)	67 (65.7)	32 (66.7)	26 (68.4)	0.954
	CMS	63 (33.5)	35 (34.3)	16 (33.3)	12 (31.6)	
Age at surgery (years), median [Q1, Q3]		5.1 [3.0,7.9]	5.3 [3.5,8.5]	5.3 [2.5,7.5]	4.3 [2.4,6.6]	0.052
Sex, n (%)	Female	75 (39.9)	41 (40.2)	19 (39.6)	15 (39.5)	0.996
	Male	113 (60.1)	61 (59.8)	29 (60.4)	23 (60.5)	
Tumors size, median [Q1, Q3]		49.6 [40.5,57.1]	49.2 [41.1,56.8]	49.0 [38.3,53.9]	54.9 [41.9,60.3]	0.411
Consistency, n (%)	Non-solid	27 (14.4)	19 (18.6)	6 (12.5)	2 (5.3)	0.122
	Solid	161 (85.6)	83 (81.4)	42 (87.5)	36 (94.7)	
Hydrocephalus, n (%)	No	98 (52.1)	52 (51.0)	23 (47.9)	23 (60.5)	0.480
	Yes	90 (47.9)	50 (49.0)	25 (52.1)	15 (39.5)	
Paraventricular edema, n (%)	No	75 (39.9)	38 (37.3)	19 (39.6)	18 (47.4)	0.553
	Yes	113 (60.1)	64 (62.7)	29 (60.4)	20 (52.6)	
Presurgical VP shunt, n (%)	No	167 (88.8)	94 (92.2)	39 (81.2)	34 (89.5)	0.140
	Yes	21 (11.2)	8 (7.8)	9 (18.8)	4 (10.5)	
EOR, n (%)	Non-GTR	25 (13.3)	12 (11.8)	11 (22.9)	2 (5.3)	0.045
	GTR	163 (86.7)	90 (88.2)	37 (77.1)	36 (94.7)	
Surgical Route, n (%)	R1	42 (22.3)	19 (18.6)	15 (31.2)	8 (21.1)	<0.001
	R2	37 (19.7)	6 (5.9)	12 (25.0)	19 (50.0)	
	*R*3	42 (22.3)	20 (19.6)	11 (22.9)	11 (28.9)	
	R4	67 (35.6)	57 (55.9)	10 (20.8)		
Pathology, n (%)	EP	24 (12.8)	9 (8.8)	4 (8.3)	11 (28.9)	0.006
	MB	74 (39.4)	47 (46.1)	19 (39.6)	8 (21.1)	
	Other	90 (47.9)	46 (45.1)	25 (52.1)	19 (50.0)	

Abbreviations: CMS = cerebellar mutism syndrome, EOR = extent of resection, GTR = gross total resection, EP = ependymoma, MB = medulloblastoma, R1 = other surgical routes, R2 = telovelar approach, *R*3 = *trans*-vermis approach, R4 = unknown approach. Note: Age and tumor sized were presented with median [Q1, Q3].

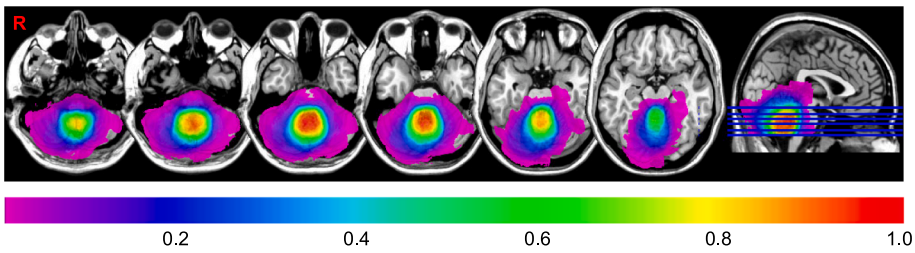

Fig. 1. The overall Lesion overlap for the training set. The whole cerebellum, fourth ventricle, and the dorsal part of the brainstem mainly in the pons are affected.

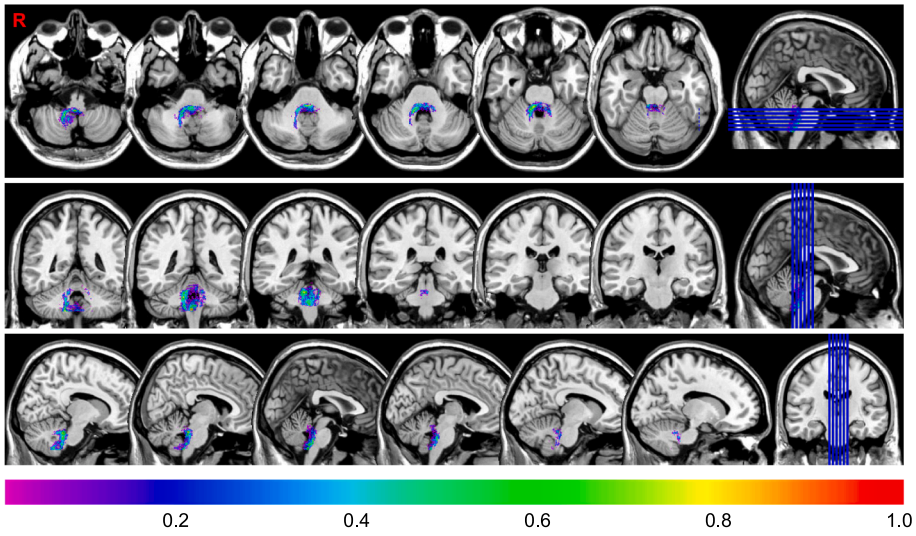

Fig. 2. Subtraction lesion map of CMS and non-CMS group. Two probability overlap maps were calculated using the number of overlaps in each voxel divided by the total number of patients in CMS (63) and non-CMS groups (1 2 5) respectively. And then the subtraction map was the subtraction of non-CMS probability overlap from CMS probability overlap. The values range from 0.2 to 0.4, which means that the percentage of affecting corresponding voxels in the CMS group is higher by 20%–40% than in the non-CMS group.

than that in non-CMS can be presented in the results.

4.2. Lesion symptom mapping and model performance

The sparseness value for the SCCAN is 0.40 with a CV correlation p value < 0.001. LESY map analysis of CMS yielded 7763 significant voxels with the peak voxel located at right cerebellum lobe VIII (MNI 21, −52, −58). Eight voxel clusters were significantly associated with CMS development, and were mainly located at right superior cerebellar peduncles, superior cerebellar lobes, and brain stem areas (Fig. 3). The largest fraction values of anatomical statistics for significant voxels are shown in Table 3. The right side of cerebellar hemisphere (significant voxels = 281), right superior (significant voxels = 129) and inferior cerebellar peduncles (significant voxels = 83) have the most significant voxels of the clusters. In the right cerebellar hemisphere, the lobule Crus I (significant voxels = 100), lobule VI (significant voxels = 68), and lobule VI_V (significant voxels = 80) had the largest significant voxels. The MNI coordinates of the centers of these clusters are listed in Table 4.

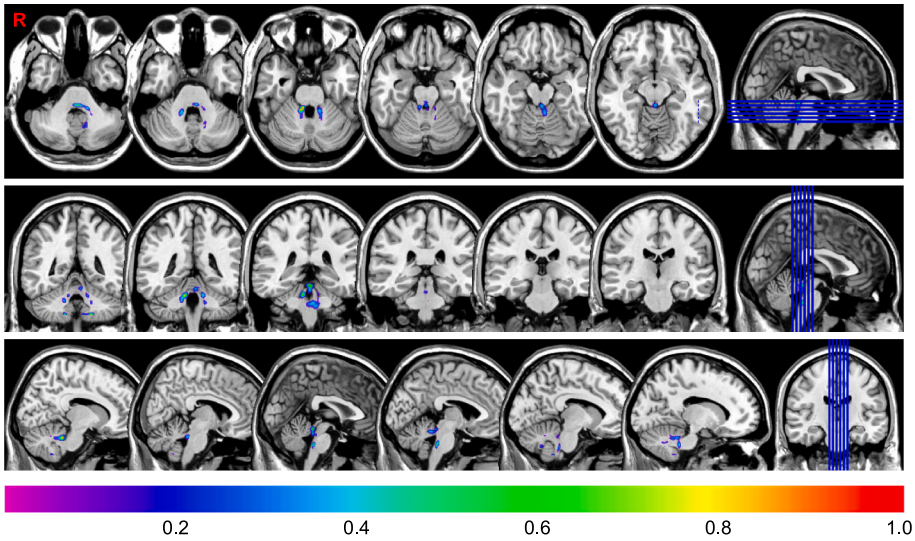

Fig. 3. The lesion-symptom mapping in axial and sagittal view for the training set. Significant voxels reside in bilateral superior and inferior cerebellar peduncles, brainstem, and superior ventral part of the cerebellum. The lesion-symptom mapping presents a right-lateralized dominance pattern.

Table 2
Comparison of CMS and non-CMS group.

		Overall (N = 188)	Non-CMS (N = 125)	CMS (N = 63)	P-Value
Age at surgery (years), median [Q1, Q3]		5.1 [3.0,7.9]	4.8 [2.9,7.8]	5.6 [3.6,8.4]	0.335
Sex, n (%)	Female	75 (39.9)	59 (47.2)	16 (25.4)	**0.006**
	Male	113 (60.1)	66 (52.8)	47 (74.6)	
Tumor volume (mm^3), median [Q1, Q3]		6934.0 [4224.5,11130.5]	7372.0 [4099.0,12797.0]	6030.0 [4399.5,9256.0]	0.557
Tumor consistency, n (%)	Non-solid	27 (14.4)	26 (20.8)	1 (1.6)	**0.001**
	Solid	161 (85.6)	99 (79.2)	62 (98.4)	
Hydrocephalus, n (%)	No	98 (52.1)	73 (58.4)	25 (39.7)	**0.023**
	Yes	90 (47.9)	52 (41.6)	38 (60.3)	
Paraventricular edema, n (%)	No	75 (39.9)	58 (46.4)	17 (27.0)	**0.016**
	Yes	113 (60.1)	67 (53.6)	46 (73.0)	
Presurgical VP shunt, n (%)	No	167 (88.8)	114 (91.2)	53 (84.1)	0.227
	Yes	21 (11.2)	11 (8.8)	10 (15.9)	
EOR, n (%)	Non-GTR	25 (13.3)	14 (11.2)	11 (17.5)	0.334
	GTR	163 (86.7)	111 (88.8)	52 (82.5)	
Surgical Route, n (%)	R1	42 (22.3)	39 (31.2)	3 (4.8)	**0.001**
	R2	37 (19.7)	21 (16.8)	16 (25.4)	
	*R*3	42 (22.3)	24 (19.2)	18 (28.6)	
	R4	67 (35.6)	41 (32.8)	26 (41.3)	
Pathology, n (%)	EP	24 (12.8)	14 (11.2)	10 (15.9)	**<0.001**
	MB	74 (39.4)	34 (27.2)	40 (63.5)	
	Other	90 (47.9)	77 (61.6)	13 (20.6)	

Abbreviations: CMS = cerebellar mutism syndrome, EOR = extent of resection, GTR = gross total resection, EP = ependymoma, MB = medulloblastoma, R1 = other surgical routes, R2 = telovelar approach, *R*3 = *trans*-vermis approach, R4 = unknown approach. Note: Age and tumor sized were presented with median [Q1, Q3].

Table 3
Detailed anatomical descriptions of the significant voxel clusters identified in VLSM analysis.

Anatomy	Nvoxels	Nsig	Intensity	Fraction	Extension	Atlas
Fibers						
Right side						
Inferior Cerebellar Peduncle	4647	83	0.69	1.79 %	14.72 %	Natbrainlab
Superior Cerebellar Peduncle	7346	129	0.67	1.76 %	22.87 %	Natbrainlab
Left side						
Superior Cerebellar Peduncle	6977	29	0.61	0.42 %	5.14 %	Natbrainlab
Inferior Cerebellar Peduncle	4881	6	0.39	0.12 %	1.06 %	Natbrainlab
Cerebellar lobes						
Left side						
Cerebellum III	1072	51	0.72	4.76 %	9.04 %	AAL
Cerebellum IV_V	9034	3	0.52	0.03 %	0.53 %	AAL
Right side						
Cerebellum VI_V	6763	80	0.64	1.18 %	14.18 %	AAL
Cerebellum Crus I	21,017	100	0.60	0.48 %	17.73 %	AAL
Cerebellum VI	14,362	68	0.61	0.47 %	12.06 %	AAL
Cerebellum IX	4635	17	0.60	0.37 %	3.01 %	AAL
Cerebellum VIII	9541	7	0.60	0.07 %	1.24 %	AAL
Cerebellum Crus II	16,804	9	0.54	0.05 %	1.60 %	AAL
Middle part						
Vermis I_II	404	15	0.61	3.71 %	2.66 %	AAL
Vermis IV_V	5324	66	0.56	1.24 %	11.70 %	AAL
Vermis III	1822	17	0.58	0.93 %	3.01 %	AAL
Vermis VI	2956	10	0.57	0.34 %	1.77 %	AAL

Abbreviations: AAL = Anatomical Automatic Labeling. Fraction represents the proportion of each ROI covered by each significant z-statistic map. Extension represents the proportion of each cluster covered by corresponding ROI. Nsig refers to the number of significant voxels within each ROI. Nvoxels refers to the total number of voxels within the corresponding ROI. The center of each cluster was represented in MNI coordinates.

4.3. Model performance

The model performance was assessed by AUC evaluation. Our voxel-wise predictive model showed good performance in the training set (AUC = 0.889) and acceptable performance in the validation (AUC = 0.784) and prospective validation (AUC = 0.791) sets (Fig. 4). The predicting accuracies of the model in training, validation and prospective validation sets were 0.83, 0.71 and 0.73 respectively.

5. Discussion

CMS attracts increasing attention due to long-term sequela in children with posterior fossa tumors. However, the mechanism underlying this clinical syndrome remains unknown. Tumor location has been demonstrated to play a significant role in CMS development. However, in previous studies, tumor location was determined by visual assessment, which is unreliable and causes information lost. Therefore, LSM, a broadly utilized tool in cognitive research, was used in this study to determine the distribution pattern of tumors leading to CMS in the MNI space. In addition, a predictive model was established based on presurgical tumor voxels. This study aimed to explore the mechanism of CMS and predict its occurrence before surgery, which would help surgeons pay more attention to the operation procedure and reduce the risk of CMS by taking appropriate measures during surgery.

In our study, the lesion map and LSM results showed a right lateralization distribution (mainly located at right lobule Crus I, lobules IV-V,

Table 4
MNI coordinates of the clusters' peak voxel and center.

Clusters	Nvoxels	Coordinate of the peak voxel			Coordinate of the cluster center		
		X	Y	Z	X	Y	Z
1	1882	75	45	32	81.4	55.6	41.5
2	1594	103	41	9	102	44.1	21
3	1580	87	73	4	86.9	71.9	18
4	1004	63	67	14	66.6	70.4	22.1
5	882	77	76	26	79.6	74.2	32.5
6	323	70	55	0	63.8	60.5	1.12
7	269	85	48	8	89.2	52.2	13.3
8	229	93	62	0	92.8	65.9	0.716

and lobule VI) of significant voxels, consistent with previous studies of cerebellar function mapping (King et al., 2019). Converging lines of image research have revealed cerebellum participates in multiple cognitive functions much more than in sensorimotor control (Ivry and Baldo, 1992). Functional MRI found that right cerebellar lobules VI-Crus I and a second cluster in lobules VIIB-VIII are associated with the language process (Ji et al., 2019; King et al., 2019; Stoodley et al., 2012), which further corroborates our findings. In addition, more direct evidence from lesion studies indicated that damage to right medial posterior cerebellum results in transient language difficulties, including verbal fluency and sentence processing (Geva et al., 2021). However, how the cerebellum contributes to language function and interacts with cortical language functional area remains unknown. The cerebrocerebellar circuit constitutes a substantial basis for the interaction between cerebrum and cerebellum. This well-known cross-walking circuit comprises the dentate nucleus, superior cerebellar peduncles, middle cerebellar peduncles and their extends, and the corresponding cerebral and cerebellar cortexes. Functional studies have revealed a cross-activation pattern (left lateral activation) between the cerebellar hemisphere and the contralateral cerebral hemisphere, which is associated with advanced cognitive function of the cerebellum (Jansen et al., 2005; Stoodley et al., 2012). Interestingly, evidence from a functional connectivity study indicates an atypical cerebrocerebellar (bilateral activation) or paradoxical activation (right lateral activation) pattern in individuals with brain tumors involving left Broca's area (Cho et al., 2018). This may be explained by contralateral reorganization for compensate of language network. We presume it may also be applied to explain the restoration of language deficits in CMS. However, a notable gap clarifying the specific mechanism of how the cerebellar is involved in language processing remains between this theory and existing

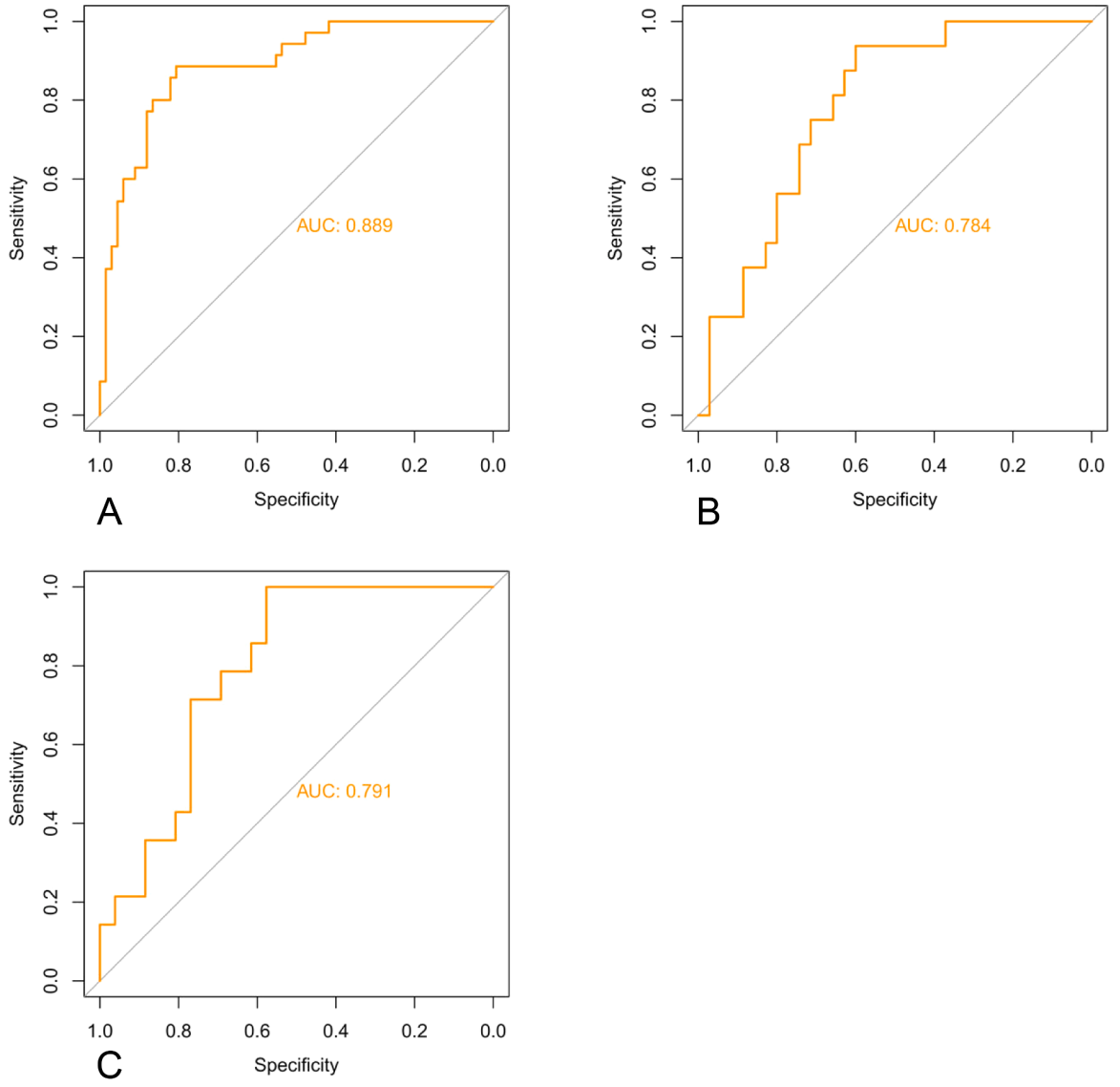

Fig. 4. The receiver operating characteristic curve of the training (A), validation set (B), and prospective sets (C).

findings.

In this study, VLSM mapping demonstrated bilateral cerebellar superior and inferior peduncles are significantly associated with CMS, especially for the right side. This corroborated, at least partially, previous studies (Gora et al., 2017; Wells et al., 2010), which identified the above risk factors for CMS. The inferior cerebellar peduncles were first identified and were thought to do with motor control (Jang and Kwon, 2016; Jossinger et al., 2020). Controversy remains regarding the laterality of superior cerebellar peduncle (SCP) damage in CMS occurrence. Previous diffusion-weighted studies have detected significant fractional anisotropy (FA) reduction in bilateral superior peduncles in CMS cases compared with non-CMS cases (Albazron et al., 2019; Avula et al., 2015; McEvoy et al., 2016; Morris et al., 2009), while others found only unilateral (right or left) impairment in SCP is associated with CMS (Law et al., 2012; Toescu et al., 2022; Vedantam et al., 2019), with fiber pathway damage lasting for a long time (McEvoy et al., 2016). Besides, no difference was detected in MCP bilaterally or unilaterally (Vedantam et al., 2019). Our findings are consistent with previous results that bilateral SCP is associated with CMS. Here we further found that the right superior cerebellar peduncle was especially involved in CMS as more massive voxels localized in the right side. However, this is inconsistent with another study, which indicated that the left superior cerebellar peduncle was associated with CMS (Toescu et al., 2022). The laterality of superior cerebellar peduncles associated with CMS still needs to be studied further. Surprisingly, bilateral dentate nuclei were not related to CMS. A possible explanation is that dentate nuclei might be protected by the surrounding fibers of middle cerebellar peduncles (MCP). In this study, therefore, both MCPs and DNs were not associated with CMS, while bilateral SCP and ICP, especially the right ones were associated with CMS.

Unlike a previous VLSM study (Albazron et al., 2019), we found that brain stem involvement was associated with CMS. This finding corroborates previous radiologic studies (Bae et al., 2020; Pettersson et al., 2022). Of note, the positive areas in VLSM results should be interpreted with caution. It is hard to determine whether these structures are infiltrated or compressed by the tumor based on VLSM, which only provides the spatial relationship of these voxels. These positive areas could be associated with CMS via tumoral involvement or surgical damage.

Previous studies have developed predictive models for CMS (Bae et al., 2020; Liu et al., 2018). However, they were based on clinical variables, and tumor locations were just divided into categories and not thoroughly utilized. In this study, a voxel-wise analysis, data driven predictive model based on VLSM for CMS was established, with reliable performance in the testing set. Compared with previous models, ours showed reliable performance in predicting CMS through tumor location alone. Furthermore, the proposed model may be used in clinic to identify the individuals vulnerable to CMS. We prospect, by exploiting the predicting model, surgeons can pay more attention to the CMS-fragile group. Previous studies have proposed several potential measurements that can reduce the incidence of CMS, such as the administration of intraoperative MR or ultrasound (El Beltagy and Atteya, 2013; Pettersson et al., 2022). By administration of intra-operative MR, ultrasound, or neurosurgical navigation, surgeons can try to spare the risky anatomical positions of CMS during the surgical process. Besides, diffusion-weighted image studies have been proven to provide visual images of neuro fibers, which could better reveal the spatial relationship between tumors and neuro fibers and facilitate the protection of cerebellar peduncles during surgery (Zhu et al., 2015). Although we have identified the risky positions for CMS, the underlying mechanism remains unclear. Functional MRI studies can provide functional connectivity changes between the cerebellum and cerebrum in CMS patients (Zhu et al., 2020), and help us better understand the mechanism of CMS. Diffusion-weighted image studies are thought to be able to quantify the injuries to neuro fibers (Zhu et al., 2015). The combination of the two MRI techniques may help researchers to uncover the mechanism of CMS and to decrease the occurrence of CMS."

There were several limitations in the current study. First, the slice thickness of the retrospectively collected MRI data was 5 mm, while the it was 1 mm in the prospective cohort. To solve the discrepancy, all masks were resampled to the same resolution and smoothed during the process of normalizing to MNI space. Secondly, this was a single center study, with no external validation from another medical center. To validate our findings, we divided our study population into the test and validation cohorts. Consequently, the sample size became relatively small after splitting. Most of the clinical features were balanced among these three groups, except for the extent of resection, the surgical route and pathology. And these unbalanced features were either unassociated with CMS in previous studies or have confounding effects with tumor location (Cobourn et al., 2020; Renne et al., 2020; Toescu et al., 2020; Yang et al., 2022). Finally, although we identified which tumor distribution pattern might induce CMS development, the findings were based on presurgical data. Other factors, especially surgical variables, which might be associated with CMS were not included in this predictive model. Another weakness of our study was that we did not include handedness in the analysis due to lacking data, as handedness was thought to be related to CMS (Law et al., 2012). Despite the above limitations, our results showed good consistency with previous reports, and the model had good performance in the validation cohorts (AUC of 0.784–0.791).

6. Conclusion

In summary, through SCCAN-based LSM, we confirmed that bilateral superior and inferior cerebellar peduncles, the superior cerebellar area, and the brain stem are associated with CMS occurrence. Besides, a presurgical predictive model for CMS based on voxel-wise level was built and the validation process revealed reliable and good performance. The identification of CMS-susceptible areas provides important insights into the etiology of CMS. Meanwhile, these findings may help clinicians take appropriate measures to prevent CMS.

7. Data availability statement

The authors confirm that the data supporting the findings of this study are available within the article and its Supplementary Material. Raw data and individual participant data cannot be made available because of ethical restrictions. Requests for access to individual participant data must be submitted to the corresponding author, and a data sharing agreement must be submitted to the University of Waterloo Office of Research Ethics.

Funding

This work was supported by the Beijing Hospital's Authority Clinical Medicine Development of Special Funding (No. XMLX202144) and the National Natural Science Foundation of China (No. 82101993).

CRediT authorship contribution statement

Wei Yang: Conceptualization, Methodology, Formal analysis, Writing – original draft, Writing – review & editing. **Yiming Li:** Software, Methodology, Formal analysis, Writing – review & editing, Funding acquisition. **Zesheng Ying:** Data curation, Resources, Investigation. **Yingjie Cai:** Data curation, Resources, Investigation. **Xiaojiao Peng:** Data curation, Resources, Investigation. **HaiLang Sun:** Conceptualization, Data curation, Resources, Investigation. **Jiashu Chen:** Data curation, Resources, Investigation. **Kaiyi Zhu:** Conceptualization, Formal analysis, Writing – review & editing. **Geli Hu:** Data curation, Writing – review & editing, Validation. **Yun Peng:** Project administration, Data curation, Writing – review & editing. **Ming Ge:** Conceptualization, Project administration, Writing – review & editing, Funding acquisition.

Declaration of Competing Interest

The authors declare that they have no known competing financial interests or personal relationships that could have appeared to influence the work reported in this paper.

Data availability

Data will be made available on request.

References

Albazron, F.M., Bruss, J., Jones, R.M., Yock, T.I., Pulsifer, M.B., Cohen, A.L., Nopoulos, P. C., Abrams, A.N., Sato, M., Boes, A.D., 2019. Pediatric postoperative cerebellar cognitive affective syndrome follows outflow pathway lesions. Neurology 93, e1561–e1571.

Ashida, R., Nazar, N., Edwards, R., Teo, M., 2021. Cerebellar mutism syndrome: An overview of the pathophysiology in relation to the cerebrocerebellar anatomy, risk factors, potential treatments, and outcomes. World Neurosurg. 153, 63–74.

Avula, S., Kumar, R., Pizer, B., Pettorini, B., Abernethy, L., Garlick, D., Mallucci, C., 2015. Diffusion abnormalities on intraoperative magnetic resonance imaging as an early predictor for the risk of posterior fossa syndrome. Neuro Oncol. 17, 614–622.

Bae, D., Mlc, V.V., Catsman-Berrevoets, C.E., 2020. Preoperative prediction of postoperative cerebellar mutism syndrome. Validation of existing MRI models and proposal of the new Rotterdam pCMS prediction model. Childs Nerv. Syst. 36, 1471–1480.

Bates, E., Wilson, S.M., Saygin, A.P., Dick, F., Sereno, M.I., Knight, R.T., Dronkers, N.F., 2003. Voxel-based lesion-symptom mapping. Nat. Neurosci. 6, 448–450.

Cámara, S., Fournier, M.C., Cordero, P., Melero, J., Robles, F., Esteso, B., Vara, M.T., Rodríguez, S., Lassaletta, Á., Budke, M., 2020. Neuropsychological profile in children with posterior fossa tumors with or without postoperative cerebellar mutism syndrome (CMS). Cerebellum 19.

Catani, M., Thiebaut de Schotten, M., 2008. A diffusion tensor imaging tractography atlas for virtual in vivo dissections. Cortex 44, 1105–1132.

Catsman-Berrevoets, C.E., Aarsen, F.K., 2010. The spectrum of neurobehavioural deficits in the Posterior Fossa Syndrome in children after cerebellar tumour surgery. Cortex 46, 933–946.

Catsman-Berrevoets, C.E., Van Dongen, H.R., Mulder, P.G., Paz y Geuze, D., Paquier, P. F., Lequin, M.H., 1999. Tumour type and size are high risk factors for the syndrome of "cerebellar" mutism and subsequent dysarthria. J. Neurol. Neurosurg. Psychiatry 67, 755–757.

Cho, N.S., Peck, K.K., Zhang, Z., Holodny, A.I., 2018. Paradoxical activation in the cerebellum during language fMRI in patients with brain tumors: Possible explanations based on neurovascular uncoupling and functional reorganization. Cerebellum 17, 286–293.

Cobourn, K., Marayati, F., Tsering, D., Ayers, O., Myseros, J.S., Magge, S.N., Oluigbo, C. O., Keating, R.F., 2020. Cerebellar mutism syndrome: Current approaches to minimize risk for CMS. Child's Nervous Syst. 36, 1171–1179.

de Haan, B., Karnath, H.O., 2018. A hitchhiker's guide to lesion-behaviour mapping. Neuropsychologia 115, 5–16.

Doxey, D., Bruce, D., Sklar, F., Swift, D., Shapiro, K., 1999. Posterior fossa syndrome: Identifiable risk factors and irreversible complications. Pediatr. Neurosurg. 31, 131–136.

El Beltagy, M.A., Atteya, M.M., 2013. The benefits of navigated intraoperative ultrasonography during resection of fourth ventricular tumors in children. Childs Nerv. Syst. 29, 1079–1088.

Geva, S., Schneider, L.M., Roberts, S., Green, D.W., Price, C.J., 2021. The effect of focal damage to the right medial posterior cerebellum on word and sentence comprehension and production. Front. Hum. Neurosci. 15, 664650.

Gora, N.K., Gupta, A., Sinha, V.D., 2017. Cerebellar mutism syndrome following midline posterior fossa tumor resection in children: an institutional experience. J. Pediatr. Neurosci. 12, 313–319.

Grieco, J.A., Abrams, A.N., Evans, C.L., Yock, T.I., Pulsifer, M.B., 2020. A comparison study assessing neuropsychological outcome of patients with post-operative pediatric cerebellar mutism syndrome and matched controls after proton radiation therapy. Child's Nervous Syst. 36.

Grønbæk, J.K., Wibroe, M., Toescu, S., Frič, R., Thomsen, B.L., Møller, L.N., Grillner, P., Gustavsson, B., Mallucci, C., Aquilina, K., Fellows, G.A., Molinari, E., Hjort, M.A., Westerholm-Ormio, M., Kiudeliene, R., Mudra, K., Hauser, P., van Baarsen, K., Hoving, E., Zipfel, J., Nysom, K., Schmiegelow, K., Sehested, A., Juhler, M., Mathiasen, R., Grønbæk, J.K., Wibroe, M., Toescu, S., Frič, R., Møller, L.N., Grillner, P., Gustavsson, B., Mallucci, C., Aquilina, K., Molinari, E., Hjort, M.A., Westerholm-Ormio, M., Kiudeliene, R., Mudra, K., Hauser, P., van Baarsen, K., Hoving, E., Zipfel, J., Nysom, K., Schmiegelow, K., Sehested, A., Juhler, M., Mathiasen, R., Kjærsgaard, M., Bøgeskov, L., Skjøth-Rasmussen, J., Hauerberg Tamm, J., Poulsgaard, L., Gudrunardottir, T., Grønbæk, S.K., Blichfeldt, A., Raben-Levetzau, F.N., Thude Callesen, M., Rathe, M., Klokker, R.B., von Oettingen, G., Mikkelsen, T., Henriksen, L.T., Cortnum, S., Tofting-Olesen, K., Karppinen, A., Solem, K., Torsvik, I.K., Mosand, A.-K., Simonsen, L.R., Ehrstedt, C., Kristiansen, I., Fritzson, K., Balestrand Haga, L., Fagerholt, H.K., Stømqvist Blixt, H., Sundgren, H., Håkansson, Y., Castor, C., Nyman, P., Wretman, A., Nilsson, P., Bjørklund, A.-C., Sabel, M., Haij, I.-L., Nilsson, F., Olausson, H., Cummings, C., Flemming, J., Afolabi, D., Phipps, K., Kamaly, I., Williams, S., Jeelani, N.u.O., McArthur, D., Wiles, E., Walker, D., Cooper, R., Fellows, G., Hoole, L., Slater, K., Kandasamy, J., McAndrew, R., McLaughlin, K., Schumann, M., Avula, S., Pizer, B., Rutkauskiene, G., Matukevicius, A., van den Abbeele, L., Markia, B., Pálmafy, B., Clausen, N., Ottosen Møller, K.M., Thomassen, H., Cappelen, J., Stensvold, E., Devennay, I., Lønnqvist, T., Nordfors, K., Lähteenmäki, P., 2021. Postoperative speech impairment and surgical approach to posterior fossa tumours in children: A prospective European multicentre cohort study. Lancet Child. Adolesc. Health 5, 814–824.

Gudrunardottir, T., Morgan, A.T., Lux, A.L., Walker, D.A., Walsh, K.S., Wells, E.M., Wisoff, J.H., Juhler, M., Schmahmann, J.D., Keating, R.F., Catsman-Berrevoets, C., 2016. Consensus paper on post-operative pediatric cerebellar mutism syndrome: The Iceland Delphi results. Childs Nerv. Syst. 32, 1195–1203.

Ivry, R.B., Baldo, J.V., 1992. Is the cerebellum involved in learning and cognition? Curr. Opin. Neurobiol. 2, 212–216.

Jang, S., Kwon, H.J.N.N.W., 2016. Connectivity of inferior cerebellar peduncle in the human brain: a diffusion tensor imaging study. 26, 439.

Jansen, A., Flöel, A., Van Randenborgh, J., Konrad, C., Rotte, M., Förster, A.F., Deppe, M., Knecht, S., 2005. Crossed cerebro-cerebellar language dominance. Hum. Brain Mapp. 24, 165–172.

Ji, J.L., Spronk, M., Kulkarni, K., Repovš, G., Anticevic, A., Cole, M.W., 2019. Mapping the human brain's cortical-subcortical functional network organization. Neuroimage 185, 35–57.

Jossinger, S., Mawase, F., Ben-Shachar, M., Shmuelof, L., 2020. Locomotor adaptation is associated with microstructural properties of the inferior cerebellar peduncle. Cerebellum 19, 370–382.

Khan, R.B., Patay, Z., Klimo, P., Huang, J., Kumar, R., Boop, F.A., Raches, D., Conklin, H. M., Sharma, R., Simmons, A., Sadighi, Z.S., Onar-Thomas, A., Gajjar, A., Robinson, G.W., 2021. Clinical features, neurologic recovery, and risk factors of postoperative posterior fossa syndrome and delayed recovery: A prospective study. Neuro Oncol. 23, 1586–1596.

Kimberg, D.Y., Coslett, H.B., Schwartz, M.F., 2007. Power in Voxel-based lesion-symptom mapping. J. Cogn. Neurosci. 19, 1067–1080.

King, M., Hernandez-Castillo, C.R., Poldrack, R.A., Ivry, R.B., Diedrichsen, J., 2019. Functional boundaries in the human cerebellum revealed by a multi-domain task battery. Nature Neurosci. 22, 1371–1378.

Korah, M.P., Esiashvili, N., Mazewski, C.M., Hudgins, R.J., Tighiouart, M., Janss, A.J., Schwaibold, F.P., Crocker, I.R., Curran Jr., W.J., Marcus Jr., R.B., 2010. Incidence, risks, and sequelae of posterior fossa syndrome in pediatric medulloblastoma. Int. J. Radiat. Oncol. Biol. Phys. 77, 106–112.

Küpeli, S., Yalçın, B., Bilginer, B., Akalan, N., Haksal, P., Büyükpamukçu, M., 2011. Posterior fossa syndrome after posterior fossa surgery in children with brain tumors. Pediatr. Blood Cancer 56, 206–210.

Law, N., Greenberg, M., Bouffet, E., Taylor, M.D., Laughlin, S., Strother, D., Fryer, C., McConnell, D., Hukin, J., Kaise, C., Wang, F., Mabbott, D.J., 2012. Clinical and neuroanatomical predictors of cerebellar mutism syndrome. Neuro Oncol. 14, 1294–1303.

Liu, J.F., Dineen, R.A., Avula, S., Chambers, T., Dutta, M., Jaspan, T., MacArthur, D.C., Howarth, S., Soria, D., Quinlan, P., Harave, S., Ong, C.C., Mallucci, C.L., Kumar, R., Pizer, B., Walker, D.A., 2018. Development of a pre-operative scoring system for predicting risk of post-operative paediatric cerebellar mutism syndrome. Br. J. Neurosurg. 32, 18–27.

McEvoy, S.D., Lee, A., Poliakov, A., Friedman, S., Shaw, D., Browd, S.R., Ellenbogen, R. G., Ojemann, J.G., Mac Donald, C.L., 2016. Longitudinal cerebellar diffusion tensor imaging changes in posterior fossa syndrome. Neuroimage Clin. 12, 582–590.

McMillan, C.T., Toledo, J.B., Avants, B.B., Cook, P.A., Wood, E.M., Suh, E., Irwin, D.J., Powers, J., Olm, C., Elman, L., McCluskey, L., Schellenberg, G.D., Lee, V.M., Trojanowski, J.Q., Van Deerlin, V.M., Grossman, M., 2014. Genetic and neuroanatomic associations in sporadic frontotemporal lobar degeneration. Neurobiol. Aging 35, 1473–1482.

Morris, E.B., Phillips, N.S., Laningham, F.H., Patay, Z., Gajjar, A., Wallace, D., Boop, F., Sanford, R., Ness, K.K., Ogg, R.J., 2009. Proximal dentatothalamocortical tract involvement in posterior fossa syndrome. Brain 132, 3087–3095.

Nachev, P., 2015. The first step in modern lesion-deficit analysis. Brain 138, e354.

Q.T. Ostrom G. Cioffi K. Waite C. Kruchko J.S. Barnholtz-Sloan CBTRUS Statistical Report: Primary Brain and Other Central Nervous System Tumors Diagnosed in the United States in 2014–2018 Neuro Oncol 23 2021 iii1-iii105.

Pettersson, S.D., Kitlinski, M., Miękisiak, G., Ali, S., Krakowiak, M., Szmuda, T., 2022. Risk factors for postoperative cerebellar mutism syndrome in pediatric patients: A systematic review and meta-analysis. J. Neurosurg. Pediatr. 29, 467–475.

Pols, S., van Veelen, M.L.C., Aarsen, F.K., Gonzalez Candel, A., Catsman-Berrevoets, C.E., 2017. Risk factors for development of postoperative cerebellar mutism syndrome in children after medulloblastoma surgery. J. Neurosurg. Pediatr. 20, 35–41.

Pustina, D., Avants, B., Faseyitan, O.K., Medaglia, J.D., Coslett, H.B., 2018. Improved accuracy of lesion to symptom mapping with multivariate sparse canonical correlations. Neuropsychologia 115, 154–166.

Renne, B., Radic, J., Agrawal, D., Albrecht, B., Bonfield, C.M., Cohrs, G., Davis, T., Gupta, A., Hebb, A.L.O., Lamberti-Pasculli, M., Knerlich-Lukoschus, F., Lindsay, S., McNeely, P.D., Pillai, S., Rai, H.I.S., Sborov, K.D., Vitali, A., Walling, S., Woerdeman, P., Suryaningtyas, W., Cochrane, D., Singhal, A., Steinbok, P., 2020. Cerebellar mutism after posterior fossa tumor resection in children: a multicenter international retrospective study to determine possible modifiable factors. Childs Nerv. Syst. 36, 1159–1169.

Robertson, P.L., Muraszko, K.M., Holmes, E.J., Sposto, R., Packer, R.J., Gajjar, A., Dias, M.S., Allen, J.C., Children's Oncology, G., 2006. Incidence and severity of postoperative cerebellar mutism syndrome in children with medulloblastoma: A prospective study by the Children's Oncology Group. J. Neurosurg. 105, 444–451.

Rolls, E.T., Huang, C.C., Lin, C.P., Feng, J., Joliot, M., 2020. Automated anatomical labelling atlas 3. Neuroimage 206, 116189.
Rudrauf, D., Mehta, S., Bruss, J., Tranel, D., Damasio, H., Grabowski, T.J., 2008. Thresholding lesion overlap difference maps: Application to category-related naming and recognition deficits. Neuroimage 41, 970–984.
Sperber, C., Karnath, H.O., 2017. Impact of correction factors in human brain lesion-behavior inference. Hum. Brain Mapp. 38, 1692–1701.
Steinbok, P., Cochrane, D.D., Perrin, R., Price, A., 2003. Mutism after posterior fossa tumour resection in children: Incomplete recovery on long-term follow-up. Pediatr. Neurosurg. 39, 179–183.
Stoodley, C.J., Valera, E.M., Schmahmann, J.D., 2012. Functional topography of the cerebellum for motor and cognitive tasks: An fMRI study. Neuroimage 59, 1560–1570.
Toescu, S.M., Hales, P.W., Aquilina, K., Clark, C.A., 2018. Quantitative MRI in post-operative paediatric cerebellar mutism syndrome. Eur. J. Radiol. 108, 43–51.
Toescu, S.M., Samarth, G., Layard Horsfall, H., Issitt, R., Margetts, B., Phipps, K.P., Jeelani, N.U., Thompson, D.N.P., Aquilina, K., 2020. Fourth ventricle tumors in children: Complications and influence of surgical approach. J. Neurosurg. Pediatr. 27, 52–61.
Toescu, S.M., Bruckert, L., Jabarkheel, R., Yecies, D., Zhang, M., Clark, C.A., Mankad, K., Aquilina, K., Grant, G.A., Feldman, H.M., Travis, K.E., Yeom, K.W., 2022. Spatiotemporal changes in along-tract profilometry of cerebellar peduncles in cerebellar mutism syndrome. NeuroImage: Clinical 35, 103000.
Vedantam, A., Stormes, K.M., Gadgil, N., Kralik, S.F., Aldave, G., Lam, S.K., 2019. Association between postoperative DTI metrics and neurological deficits after posterior fossa tumor resection in children. J. Neurosurg. Pediatr. 1–7.
Wells, E.M., Khademian, Z.P., Walsh, K.S., Vezina, G., Sposto, R., Keating, R.F., Packer, R.J., 2010. Postoperative cerebellar mutism syndrome following treatment of medulloblastoma: Neuroradiographic features and origin. J. Neurosurg. Pediatr. 5, 329–334.
Wibroe, M., Ingersgaard, M.V., Larsen, H.B., Juhler, M., Piil, K., 2021. Living with the cerebellar mutism syndrome: Long-term challenges of the diagnosis. Acta Neurochir (Wien) 163, 1291–1298.
Yang, W., Ge, M., Zhu, K., Chen, J., Yang, P., Cai, Y., Peng, X., Wang, J., Sun, H., Ji, Y., Zhao, F., Zhang, H., 2022. Male predisposition in cerebellar mutism syndrome: A cohort study. Cerebellum.
Zhang, Y., Kimberg, D.Y., Coslett, H.B., Schwartz, M.F., Wang, Z., 2014. Multivariate lesion-symptom mapping using support vector regression. Hum. Brain Mapp. 35, 5861–5876.
Zhu, D.M., Yang, Y., Zhang, Y., Wang, C., Wang, Y., Zhang, C., Zhao, W., Zhu, J., 2020. Cerebellar-cerebral dynamic functional connectivity alterations in major depressive disorder. J. Affect Disord. 275, 319–328.
Zhu, J., Zhuo, C., Qin, W., Wang, D., Ma, X., Zhou, Y., Yu, C., 2015. Performances of diffusion kurtosis imaging and diffusion tensor imaging in detecting white matter abnormality in schizophrenia. Neuroimage Clin. 7, 170–176.